Polymer Journal (2018) 50:679–687
https://doi.org/10.1038/s41428-018-0066-2

FOCUS REVIEW

Application of a polarized modulation technique in supramolecular science: chiroptical measurements of optically anisotropic systems

Takunori Harada[1]

Received: 18 January 2018 / Revised: 7 April 2018 / Accepted: 9 April 2018 / Published online: 21 May 2018

Abstract

The chirality of a supramolecular assembly provides particularly valuable information because the bonding nature of noncovalent interactions, such as electrostatic interactions, π effects, van der Waals forces, and hydrophobic effects, makes the development of supramolecular assemblies an attractive and useful approach in chiral induction, chiral amplification, and chirality transfer. However, chiroptical measurements of optically anisotropic samples cannot be generally achieved with modern chiroptical spectrophotometric methods such as circular dichroism (CD) or circular birefringence (CB) and circularly polarized luminescence (CPL) that are based on polarization modulation techniques because of the coupling effect of the nonideal optics and the electronics with strong macroscopic anisotropies, that is, nonchiral signals related to linearly polarized phenomena. These artifact signals are often much stronger than the chiroptical signals. Only CD and CPL spectrophotometers developed in 2001 and 2016, respectively, and integrated into a Stokes–Mueller matrix analysis for optically anisotropic samples are capable of obtaining accurate chirality measurements of samples with macroscopic anisotropies. Therefore, these spectrophotometers enable chiral investigations of optically anisotropic samples, for example, single crystals, supramolecular assemblies, gels, films, membranes, polymers, and liquid crystals. This focus review presents a short and elementary discussion of the chiroptical measurement techniques for optically anisotropic samples in supramolecular science and signal interpretation in polarization spectroscopy.

Introduction

Chiroptical analysis, for example, of the electronic optical activity (EOA), is important in the study of chirality. It consists of two major subfields, absorptional circular dichroism (CD) and circularly polarized luminescence (CPL), for the differential absorption and emission of left circularly polarized vs. right circularly polarized radiation in chiral molecules. Well-known chiroptical techniques for the measurement of chirality are electronic CD (ECD) and CPL spectroscopies; other techniques include vibrational CD [1] (VCD), circular birefringence (CB ≡ optical rotational dispersion (ORD)), and diffuse reflection [2] and scattering [3]. ECD [4] and CPL [5] were reported and independently confirmed approximately 80 years ago. Since then, there have been many advances in the instrumentation [6], theory [7, 8], calculations [9], and applications of EOA. In particular, the commercially available ECD instruments based on the polarization modulation technique developed in the 1960s and the CPL instruments developed in 1983 [10] opened EOA to scientists interested in analyzing the molecular structure of chiral molecules. Today, EOA applications continue to expand, for example, in the widespread use of ECD for the determination of the absolute configuration of pharmaceutical and natural product molecules and the determination of enantiomeric excess in molecules with ultraviolet–visible light (UV–vis) chromophores and fluorophores. In particular, chiral chemistry has been widely studied in the solid state rather than the solution state because molecular recognition/discrimination, chiral transcription, and chiral amplification are significant in the solid state as a result of the short distance between adjacent molecules. Chiroptical measurements of optically active samples with macroscopic anisotropy have advanced

✉ Takunori Harada
tharada@oita-u.ac.jp

[1] Department of Integrated Science and Technology, Faculty of Science and Technology, Oita University, Dannoharu, 700, Oita city 870-1192, Japan

significantly since the discovery of solid-state CD in 1969 by McCaffery and co-workers [11]. We do not doubt that true chirality measurements of CD and CPL signals are of utmost importance. However, the standard CD and CPL applications are severely restricted to the analysis of optically isotropic materials because the chiroptical spectra measured by polarization modulation spectroscopy are necessarily accompanied by artifacts due to macroscopic anisotropies, that is, in films [12, 13], gels [14], liquid crystals [15, 16], polymers [17], and supramolecular compounds such as self-assemblies [18, 19], even in the solution state, wherein molecules are generally considered to be anisotropy-free. Norden [20], Jensen et al. [6], Dekkers et al. [21], Shindo and Ohmi [22], and Shindo and Oda [23]. demonstrated the instrumental limitations of CD and CPL spectrometers in the study of the CD and CPL phenomena of samples with macroscopic anisotropy, and the usefulness of the Stokes–Mueller matrix for analyzing the data was demonstrated. However, the very important papers by these authors are frequently overlooked. Thus, the measurement of chiroptical properties, that is, the CD and CPL signals, using commercially available chiroptical spectrophotometers is extremely difficult in the solid and condensed phases for optically anisotropic cases. We essentially need special circumstances, except in optically homogeneous cases, to analyze the directly obtained spectra, which inevitably suffer from artifacts resulting from the interaction between the macroscopic anisotropies of a sample (i.e., the linear birefringence (LB), linear dichroism (LD), and linearly polarized luminescence (LPL)) and the nonideal characteristics of the polarization modulation instruments [24].

In 2001, Kuroda, Harada and Shindo designed and constructed a solid-state CD spectrophotometer and an analytical procedure based on the Stokes–Mueller matrix [25] that are capable of measuring the artifact-free CD and CB spectra of optically anisotropic samples, including optically inhomogeneous materials [26–29]. The solid-state dedicated chiroptical spectrophotometer (universal chiroptical spectrophotometer (UCS)) has provided valuable information about solid-state structures and supramolecular properties that are not obtainable from the solution phase [30] (and the references therein). Details of the instrumentation and applications with chiral materials are discussed in later sections.

CPL spectroscopy is a well-known technique for studying the stereochemical, conformational, and three-dimensional structures of chiral molecules in their excited states. This technique can be considered the emission counterpart of ECD, which occurs during absorption, and the two techniques are complementary chiroptical tools for probing the excited-state and ground-state structures of chiral entities. CPL is also a popular tool for the study of chirality because CPL spectroscopy has found many intriguing applications, such as in sensing the chirality of biomolecules [31], polarized light sources (supramolecular assemblies [32, 33], liquid crystals [34] (and the references therein), [35], and polymers [36]), smart memory materials with photochemically switchable CPL properties[37], circularly polarized electroluminescence [38], and optoelectronic devices [39]. Similarly, conventional CPL measurements have thus far been restricted to cases where the orientational distribution of the emitting molecules is isotropic with no photoselection; acquisition of the true CPL signal in the condensed phase is very difficult except in special homogeneous cases. Moreover, researchers determined that the measurement of the LPL signal was critical for achieving artifact-free CPL measurements using a theoretical analysis except in the case of fluorophore molecules in an isotropic medium or the measurement of a crystal along its unique optical axis, where the CPL signal is free from anisotropic effects [40]. In 2012, an analytical procedure for obtaining artifact-free CPL spectra was theoretically derived on the basis of the Stokes–Mueller matrix approach [40], and a new CPL spectrophotometer based on this theoretical analysis was devised; this spectrophotometer was named the comprehensive chiroptical spectrophotometer (CCS: J-700CPL) [41] because of its ability to measure all true polarization phenomena, including absorption and emission events. This focus review presents a discussion of the chiroptical measurement techniques for optically anisotropic samples whose dimensions range from nanometers to micrometers in supramolecular science and signal interpretation in polarization spectroscopy.

Materials and methods

To obtain true chiroptical signals from optically anisotropic samples, a dedicated solid-state UCS [26] has been designed and constructed by using the Stokes–Mueller matrix method, which is particularly effective in understanding the physical meaning of signals observed in polarization modulation spectroscopy and in evaluating an instrument's performance. Figure 1 shows the optical system of the first-generation UCS or CCS and the axis orientations of the optical and electrical components. The UCS consists of a 450-W Xe arc lamp, double-prism monochromator, polarizer consisting of a stack of plates and a photoelastic modulator (PEM) in a CD spectrometer (J-series: JASCO, Tokyo, Japan), sample stage, sample holder, Glan–Taylor polarizing prism, Hamamatsu R-376 head-on-type photomultiplier (PM), lamp and PM power supply from JASCO (Tokyo, Japan), and two 50-kHz and 100-kHz lock-in amplifiers (LIAs) [26].

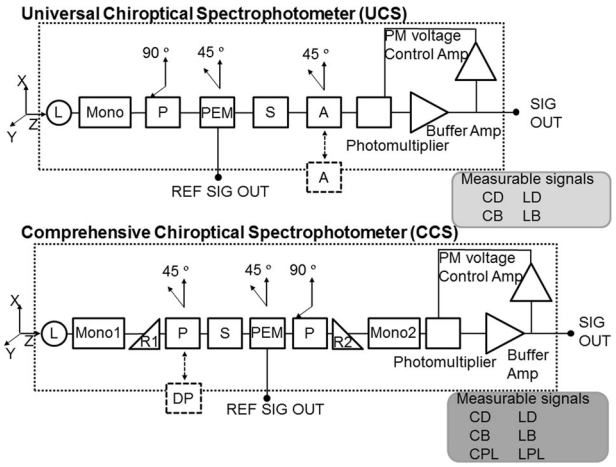

Fig. 1 Block diagrams of the universal chiroptical spectrophotometer (UCS) and comprehensive chiroptical spectrophotometer (CCS). L light source, Mono monochromator, P polarizer, R right-angle prism, DP depolarizer, PEM photoelastic modulator, S sample, A analyzer, and PM photomultiplier. The condenser and collimator lenses are omitted for clarity

The novel CCS instrument is equipped with right-angle prisms and a horizontal sample stage. The CCS can provide artifact-free CD spectra by removing the substantial artifact signals that are intrinsic to macroscopically anisotropic condensed phases. Moreover, the instrument was designed to measure the CPL and CD. The CCS system consists of a 450-W Xe arc lamp, grating monochromator (JASCO, Tokyo, Japan), right-angle prisms (RPSQ-25-10H, SIGMA KOKI Co., Ltd., Tokyo, Japan), depolarizer (PDH15, B. Halle Nachfl. GmbH, Germany), polarizer (quartz plates arranged at Brewster's angle), sample stage (SGSP-60YAW-0B, SIGMA KOKI Co., Ltd., Tokyo, Japan), sample holder, Hamamatsu R-376 head-on type PM, lamp and PM power supply (JASCO, Tokyo, Japan), and LIA (JASCO, Tokyo, Japan) [41]. The output from the PM is a DC signal superimposed by modulated AC components. For the CD measurements, the DC level is maintained at a constant value (500 mV), independent of the total amount of light, via the servo control of a PM power supply through the feedback of the DC component; in the case of the CPL, the high tension (HT) voltage is maintained at an arbitrary value. The signal processing is set up to record the ratio of the AC signals to the DC signals. The electrical signals processed by the 50-kHz and 100-kHz LIAs are transmitted to a PC. The rotational LPL and LD signals are obtained at 513 and 450 nm by the computer-controlled rotation of a sample by 360° in the *x*–*y* plane at speeds of 1.25° and 2.5°/s, respectively.

Benzil (PhCOCOPh) and 5,10,15,20-tetrakis(4-sulfonatophenyl)porphyrin (TPPS) were purchased from STREM Chemical Inc. (MA, USA) and Wako Pure Chemical Industries (Tokyo, Japan), respectively. The cationic surfactants cetyltrimethylammonium bromide (CTAB) and (–)-(1*R*, 2*S*)-*N*-dodecyl-*N*-methylephedrinium bromide (DMEB) were purchased from Sigma-Aldrich Co. Ltd. (Tokyo, Japan). (+)-DMEB was prepared at an overall yield of 53% from (1*S*, 2*R*)-(+)-norephedrine using a previously reported method [42]. Both (-)-DMEB and (+)-DMEB were used without further purification. Benzil was recrystallized from ether. Benzil molecules exhibit optical activity only in the crystalline state because of their chiral supramolecular arrangement of nonchiral components. The single crystal belongs to the trigonal–trapezohedral symmetry class with the space group $P3_121$ or $P3_221$. Single crystals up to 5 mm in size were grown from saturated solutions in hexagonal form. The crystals were polished to make a plate with a thickness of 45–50 μm perpendicular to either the right-handed or left-handed threefold screw axis.

Theory

The Stokes–Mueller matrix method was employed in the experiments. The Stokes vector $S = [S_0, S_1, S_2, S_3]$ [43, 44] is useful for expressing the polarization states of light, where S_0, S_1, S_2, and S_3 denote the total intensity, plus 45° preference, right circular preference, and horizontal preference of light, respectively. The Mueller matrix [45, 46] is the 4×4 matrix $\mathbf{S} = M_{ij}$ that was devised to express the optical characteristics of optical elements and samples, and the detailed elements M_{ij} are described below. In the UCS, from a simple calculation of the Stokes–Mueller matrix, $\mathbf{D \cdot L_2 \cdot S \cdot L_1 \cdot M_{(45,\delta)} \cdot P_{(90)} \cdot Mo \cdot L_0 \cdot I_0}$, we obtain the AC signals detected by the 50 kHz LIA as [26]

$$\begin{aligned}\text{Signal}_{\text{AC}} = {} & G_1\left(P_x^2 + P_y^2\right)[(\text{CD} + 1/2(\text{LB}'\text{LD} - \text{LBLD}')] \\ & + G_1\left(P_x^2 - P_y^2\right)\sin 2a\,(-\text{LB}\cos 2\theta + \text{LB}'\sin 2\theta),\end{aligned} \tag{1}$$

where G_1 is the apparatus constant related to the sensitivity of the spectrometer at 50 kHz, P_x and P_y are the transmittance of the PM along the *x* and *y* axes, and *a* is the azimuthal angle of the optical axis with respect to the *x* axis. Furthermore, LB, LD, LB′, and LD ′ are the (*x*–*y*) LB, (*x*–*y*) LD, 45° LB, and 45° LD, respectively.

In the CCS, the AC signals detected by the 50-kHz LIA can be calculated from the matrix product of $\mathbf{D \cdot L_4 \cdot Mo \cdot L_3 \cdot P_{(90)} \cdot M_{(45,\delta)} \cdot L_2 \cdot S \cdot L_1 \cdot DP \cdot Mo \cdot L_0 \cdot I_0}$ as [41]

$$\text{Signal}_{50\,\text{kHz}} = G'_1[(M_{20}) + (\text{LB}_{L2} + \sin\alpha)(M_{10})], \tag{2}$$

where G'_1 is an apparatus constant related to the LIA gain at 50 kHz and M_{10} and M_{20} are CD + 1/2(LB′LD − LBLD′

and LD′ cos 2θ + LD sin 2θ, respectively. Thus, the 50-kHz signal contains the CD and 1/2(LB′LD − LBLD′) signals, which are independent of the rotation of the sample, and the LD and LD′ signals multiplied by the intrinsic birefringence of the PEM or lens terms; the 50-kHz signal at an arbitrary wavelength changes with θ during sample rotation.

If the contribution of sin α is much larger than that of LB_{L2}, Eq. (2) can be approximated as

$$\begin{aligned}\text{Signal}_{50\,\text{kHz}} = G'_1[(\text{CD} + 1/2(\text{LB}'\text{LD} - \text{LBLD}') \\ +(\text{LD}'\cos 2\theta + \text{LD}\sin 2\theta)\sin\alpha].\end{aligned} \tag{3}$$

If the contribution of LB_{L2} is much larger than that of sin α, Eq. (2) can be approximated as

$$\begin{aligned}\text{Signal}_{50\,\text{kHz}} = G'_1[(\text{CD} + 1/2(\text{LB}'\text{LD} - \text{LBLD}') \\ +(\text{LD}'\cos 2\theta + \text{LD}\sin 2\theta)\text{LB}_{L2}].\end{aligned} \tag{4}$$

Since the CD signal is usually 10^2–10^3 times smaller than the LB (LB′) and LD (LD′) signals and is thus buried under the large macroscopic anisotropy signals, it is difficult to detect. However, we have observed that the following set of measurements enables the detection of the CD signal. The sample was rotated 45° from the LD_{max} position, at which the LD value becomes zero and the LD′ value reaches its maximum. At the LD′ maximum position, $\text{Signal}_{50\ \text{kHz}}$ of the face side becomes

$$[\text{Signal}_{50\,\text{kHz}}]_{\text{face}} = G'_1[(\text{CD} - 1/2\,\text{LBLD}' + \text{LD}'_{\max}\sin\alpha]$$

or

$$[\text{Signal}_{50\,\text{kHz}}]_{\text{face}} = G'_1[(\text{CD} - 1/2\,\text{LBLD}' + \text{LD}'_{\max}\text{LB}_{L2}]. \tag{5}$$

Then, the sample was rotated by 180° about the *y*-axis, which corresponds to the backside measurement. With this rotation, the CD and LD do not change signs, but LD′ becomes −LD′. Hence, the apparent CD signal of the backside becomes

$$[\text{Signal}_{50\,\text{kHz}}]_{\text{back}} = G'_1[(\text{CD} + 1/2\,\text{LBLD}' - \text{LD}'_{\max}\sin\alpha]$$

or

$$[\text{Signal}_{50\,\text{kHz}}]_{\text{back}} = G'_1[(\text{CD} + 1/2\,\text{LBLD}' - \text{LD}'_{\max}\text{LB}_{L2}]. \tag{6}$$

Thus, if we average the $[\text{Signal}_{50\,\text{kHz}}]_{\text{face}}$ and $[\text{Signal}_{50\,\text{kHz}}]_{\text{back}}$ spectra, we obtain the true CD spectrum. Similarly, with our set of procedures based on the Stokes–Mueller matrix approach, artifact-free CD spectra can be obtained using a fine-tuned CCS spectrophotometer. The method is best applied when the artifact signals are <~30°.

We next consider an optically active material with macroscopic anisotropies and a fluorescent sample whose optical axis is not identical to that of the electronic absorption. In this case, Eq. (2) can be rewritten as

$$\begin{aligned}\text{Signal}_{50\,\text{kHz}} = G'_1\Big[\sin\alpha\left(\text{LPL}'^2 + \text{LPL}^2\right)^{1/2}\sin(2\theta' + \eta) - \text{CPL} \\ +\text{LB}'_{L2}\left(\text{LPL}'^2 + \text{LPL}^2\right)^{1/2}\sin(2\theta' - \gamma)\Big],\end{aligned} \tag{7}$$

where LPL (=$F_{0°}$−$F_{90°}$) and LPL′ (=$F_{45°}$−$F_{135°}$) are the (*x*–*y*) LPL and the 45° LPL, respectively, $\eta = \tan^{-1}$[LPL′/LPL] and $\gamma = \tan^{-1}$[LPL/LPL′]. The 50-kHz signal contains the CPL signal and the LPL and LPL′ signals multiplied by the intrinsic birefringence of the PEM or lens terms; the 50-kHz signal at an arbitrary wavelength changes with θ′ during sample rotation. If the contribution of sin α is much larger than that of LB'_{L2}, the signal changes with a periodicity of cos 2θ′. Eq. (7) can be approximated as

$$\text{Signal}_{50\,\text{kHz}} = G'_1\Big[-\text{CPL} + \sin\alpha\left(\text{LPL}'^2 + \text{LPL}^2\right)^{1/2}\sin(2\theta' + \eta)\Big]. \tag{8}$$

If the contribution of LB'_{L2} is much larger than that of sin α, Eq. (7) can be approximated as

$$\text{Signal}_{50\,\text{kHz}} = G'_1\Big[-\text{CPL} + \text{LB}'_{L2}\left(\text{LPL}'^2 + \text{LPL}^2\right)^{1/2}\sin(2\theta' - \gamma)\Big]. \tag{9}$$

We have observed that the following set of measurements makes this approximation possible. At its (+) $\text{LPL}_{\max}$ position obtained from the analysis of the 100-kHz rotational signal in Eq. (13) below, $\text{Signal}_{50\,\text{kHz}}$ becomes

$$(+)\max\,[\text{Signal}_{50\,\text{kHz}}] = G'_1[-\text{CPL} + \text{LPL}\sin\alpha]$$

or

$$(+)\max\,[\text{Signal}_{50\,\text{kHz}}] = G'_1[-\text{CPL} + \text{LPLLB}'_{L2}]. \tag{10}$$

At the negative maximum position or at the position rotated 90° from the positive maximum position, if the signal changes with a periodicity of sin 2θ′, the detected signal is given by

$$(-)\max\,[\text{Signal}_{50\,\text{kHz}}] = G'_1[-\text{CPL} - \text{LPL}\sin\alpha]$$

or

$$(-)\max\,[\text{Signal}_{50\,\text{kHz}}] = G'_1[-\text{CPL} - \text{LPL}\,\text{LB}'_{L2}]. \tag{11}$$

Thus, if we average the (+) and (−)max $[\text{Signal}_{50\ \text{kHz}}]$ spectra, we obtain the CPL. With our set of procedures based on the Stokes–Mueller matrix approach, artifact-free CPL spectra can be obtained using a specially fine-tuned CPL spectrophotometer.

Similarly, the 100-kHz component of the photocurrent detected by the LIA is given as

$$\text{Signal}_{100\,\text{kHz}} = G'_2[-(\text{LPL}'\cos 2\theta' + \text{LPL}\sin 2\theta') - \text{CPL}\sin\alpha]. \quad (12)$$

In the same way that the 50-kHz signal was approximated, Eq. (12) can be approximated as

$$\text{Signal}_{100\,\text{kHz}} = G'_2\left[-\left(\text{LPL}'^2 + \text{LPL}^2\right)^{1/2}\sin(2\theta' + \eta)\right], \quad (13)$$

where G'_2 is the apparatus constant related to the sensitivity of the spectrometer at 100 kHz. Our acquisition approach for solid-state CPL analysis largely reduces the measurement time of a dataset by ~98% compared with the time required when using our previous method [40]. It takes a short time to obtain the essential LPL axis, that is, $\pm\text{LPL}_{\text{max}}$, for solid-state CPL analysis directly from the 100-kHz signal, as explained by Eq. (13), unlike the time-consuming signal analysis performed from the 50-kHz signal (Eq. (7)) in our previous method [40].

Results

Supramolecular assemblies [47], functional polymers [48, 49], biopolymers [50–52], and so on whose dimensions are comparable to the wavelength of the irradiating probe light are optically anisotropic. Thus, it is essential to perform an analysis to discriminate the artifact signals intrinsically involved in the polarization modulation measurements regardless of the state of the components in the system, that is, the solid state (KBr matrix [53, 54], crystal [30, 55], and film [56]) or solution [57, 58]. The following are examples of chiroptical measurements of supramolecular assemblies. The chiroptical properties of water-soluble deprotonated 4-sulfonatophenyl *meso*-substituted porphyrin (TPPS) (Fig. 2) have been extensively studied by several research groups owing to the compound's unique chiral aggregation behavior in an acidic solution and the solid state. At concentrations $>1 \times 10^{-5}$ M, TPPS (H_4TPPS^{2-} dianion) molecules in an acidic aqueous solution form chiral *J*-aggregates ($(TPPS)_n$), which exhibit a quite narrow Soret band ($B_J \approx 489$ nm) attributed to the formation of intermolecular interactions between transition dipole moments, causing delocalization of the excitons over the aggregates [59]. The driving force for the formation of aggregates is intermolecular interaction between the positively charged center of the diprotonated porphyrin ring and the negatively charged peripheral sulfo groups of another H_4TPPS^{2-} molecule [60]. Immobilization of supramolecular chiral TPPS homoassociates was carried out at the air–water interface by imprinting into a quartz substrate and mediated by the electrostatic interactions between the anionic TPPS molecules and the cationic surfactant monolayer (Fig. 2). The $(TPPS)_n$/DMEB or CTAB Langmuir–Blodgett (L–B) films were examined by using a UCS [56]. Representative results for a $(TPPS)_n$/CTAB L–B film are presented in Fig. 3. Figure 3a shows the rotational measurements of the CD, LB, and LD signals at 490 nm, which is the wavelength of maximum absorbance, upon rotating the film in the *x*–*y* plane. The intensity of the CD signal dramatically changed upon sample rotation, where its shape is a trigonometric function of 2θ (Eq. (1)) and is strongly influenced by the LB and LD signals. Judging from the LB and LD rotational measurements, it was estimated that the LB and LD signals were approximately two orders of magnitude larger than the true CD signals, and the elongated axis (=LB) was almost parallel to the electric dipole transition moment defined along the LD axis. To obtain the artifact-free CD spectrum, we had to carefully analyze the measured CD spectrum using a specially devised Stokes–Mueller matrix approach [26, 30, 61] for optically anisotropic samples to remove parasitic nonchiral signals. The LB and LD values changed upon rotation non-concomitantly with the HT voltage, for example, the electronic absorption signal. Thus, the uneven film thickness and the specimen anisotropy must be the origins of these changes. It is clear from these results and from Eq. (1) that the LB and LD coupling effect substantially contributes to the CD signals. Figure 3b presents the apparent CD spectra (dotted lines) of the $(TPPS)_n$/CTAB L–B film at the LB_{max} and LB_{min} positions obtained from the rotational-dependent LB signal at the maximum absorption wavelength of 490 nm (Fig. 3a). Surprisingly, the obtained CD spectra are quite different depending on the rotational position of the sample. The spectral differences must originate from the substantial artifacts, which are mainly the coupling effect between the nonideal characteristics of the instrument and the macroscopic anisotropies, LD and LB. True CD spectra (Fig. 3b, solid line) can be obtained by employing our Stokes–Mueller matrix equation to remove the parasitic artifacts, and the resulting spectra were consistent with the results independently measured by using the CCS (see the Theory section). The interaction of TPPS with the chiral surfactant produces negatively and positively induced chiralities for (−)-DMEB and (+)-DMEB (negative and positive bisignate CD) that correspond to the left-handed or right-handed interporphyrin screw structure, which is in accordance with the exciton chirality method (Fig. 3b, inset), although the handedness of the CD signals was governed by statistical laws when achiral CTAB was employed as an amphiphile [56]. Therefore, a right-handed interporphyrin screw structure was formed in the $(TPPS)_n$/CTAB L–B film. For the CD measurement of samples with possible macroscopic anisotropies, it is necessary for the optically anisotropic system to [1] select an optically homogeneous sample carefully on the basis of the evidence

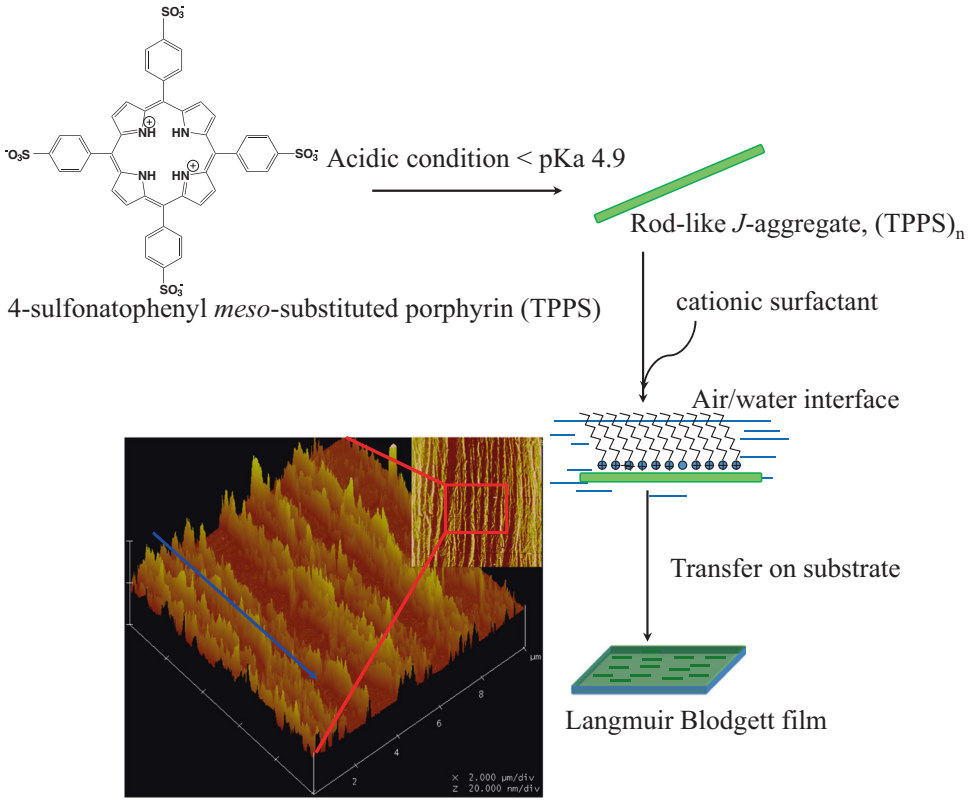

Fig. 2 Reaction route for preparing a $(TPPS)_n$-surfactant Langmuir–Blodgett film. Tapping-mode AFM image of a TPPS Langmuir–Blodgett monolayer with a surfactant transferred at a constant surface pressure (27 mN/m) to freshly cleaved mica. Arrows indicate the dipping direction in the fabrication process of the Langmuir–Blodgett film. Scales are (right) $30 \times 30\ \mu m^2$ and (left) $10 \times 10\ \mu m^2$. Reproduced with permission from Ref. 56 © 2013 OSA publishing

that the change in the HT voltage in the rotational measurements is less than 10 V; [2] measure the anisotropies (LB and LD) of the sample and the nonideal characteristics of the instrument, such as the residual static birefringence and the polarization characteristics of the optical elements in the spectrophotometer; [3] estimate the artifact signals originating from the anisotropies of the sample and the nonideal characteristics; and [4] remove these signals from the apparent CD signal using the UCS or CCS based on the specific Stokes–Mueller matrix analysis for the solid sample or using a spectrophotometer having performance equivalent to that of the UCS or CCS, except for the CD signal, which should be sufficiently large compared with any artifact signal. In the other cases of biopolymers [50, 51] in the condensed phase, the validity of the aforementioned four-step screening procedure for obtaining true chiroptical signals has also been confirmed by the Kramers–Kronig relationship between the obtained CD and CB signals. My long experience with CD measurements of optically anisotropic system indicates that if we use the above four-step screening process for optically anisotropic samples, the true CD spectrum can be obtained. Several reports demonstrate the useful application of CD spectroscopy to these types of samples, including organic gelators [62] and functional polymers such as PFs [48] and PPVs [49], among others [63].

Similarly, artifact-free CPL measurements of benzil crystals with macroscopic anisotropies were performed using a CCS and the Stokes–Mueller matrix analysis for CPL samples (see the Theory section) [40, 41]. Figure 4a shows the rotational measurements of the LPL signals at 513 nm during the rotation of a single crystal (50-μm-thick) belonging to the $P3_121$ space group placed with the crystal face perpendicular to the threefold screw axis. When the crystal was mounted slightly tilted from the perpendicular orientation, a strong LPL signal with $\sin 2\theta$ periodicity (as explained by Eq. (13)) was detected (Fig. 4a), although no LPL signal was observed when the light was incident upon the crystal exactly parallel to its axis (data not shown). The DC voltages (=nonpolarized fluorescence) changed very little upon sample rotation, and the macroscopic optical axes at the face side of the crystal closely coincided in position with those at the backside; thus, the crystals were optically homogeneous and exhibited a uniform thickness. Rotational measurements of other enantiomeric crystals were also conducted in the same manner.

To remove parasitic artifacts, true CPL spectra were carefully collected by using a Stokes–Mueller matrix analysis. Different signs of the CPL signals were obtained, even for the same sample at different positions (Fig. 4b, dotted lines). The apparent CPL spectra having near mirror images were not accurate, as they contained a parasitic signal related to the coupling effect between the macroscopic anisotropies and the nonideal characteristics, that is, the intrinsic birefringence of the collimator lens or PEM. In

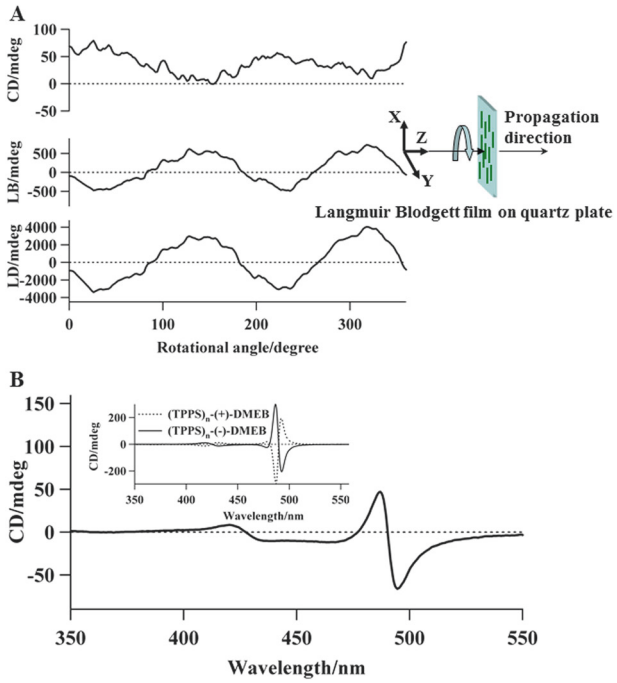

Fig. 3 **a** Changes in the CD, LB, LD, and HT signals at 490 nm of a $(TPPS)_n$/CTAB Langmuir–Blodgett (L–B) film transferred at 27 mN/m onto a quartz substrate during *X*–*Y* plane rotation. **b** True and apparent CD spectra of the $(TPPS)_n$/CTAB L–B film. The inset shows the CD spectra of the $(TPPS)_n$/(+)-DMEB (dotted line) and (−)-DMEB (solid line) complexes in an acidic aqueous solution (pH = 2.3); [TPPS] = 0.01 mM, [(+)-DMEB and (−)-DMEB] = 0.01 mM. Reproduced with permission from Ref. 56 © 2013 OSA publishing

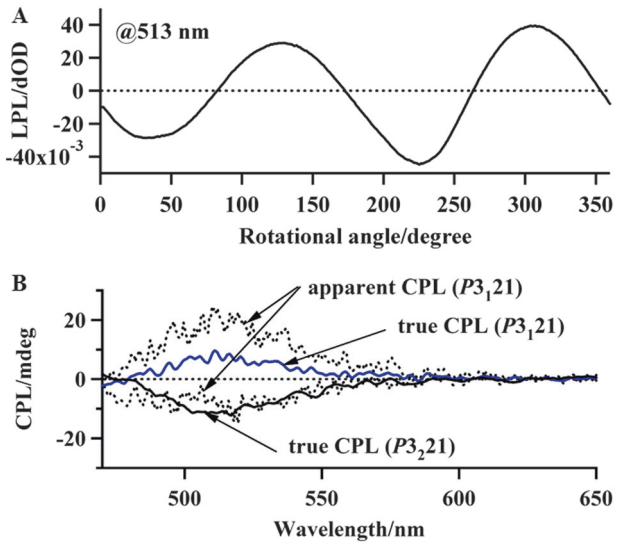

Fig. 4 **a** LPL rotational signals at 513 nm of a benzil single crystal ($P3_121$, 50-μm-thick) that is slightly tilted from the perpendicular orientation. **b** True (solid line) and apparent (dotted line) CPL spectra of a benzil crystal ($P3_121$) and true CPL (solid line) spectrum of an isomer $P3_221$ crystal (45-μm-thick), as obtained from a Stokes–Mueller matrix analysis of optically anisotropic samples; the excitation wavelength, λ_{ex}, is 360 nm, and the absolute value of g_{lum} is 0.002 at 513 nm. Reproduced with permission from Ref. 41 © 2016 AIP publishing

this case, the absolute maximum artifact signal (i.e., the LPL term multiplied by the nonideal characteristics (sinα or LB'_{L2})) was estimated to be 2.6×10^{-4} dOD (approximately equal to 8.7 mdeg) from the LPL and apparent CPL signals shown in Fig. 4a, b. The term multiplied by $\sin\alpha$ in Eq. (7) is larger than LB'_{L2} because the residual static birefringence, α, of our instrument is −0.36° at 500 nm, that is, $\sin\alpha$ is -6.25×10^{-3}, and the intrinsic birefringence of the collimator lens, LB'_{L2}, is on the order of 2×10^{-3}. Thus, the 50-kHz signal can be approximated as Eq. (8). By adopting the devised procedure, artifact-free CPL spectra (Fig. 4b, solid line) could be obtained by averaging the apparent CPL spectra at the angular positions of $\pm LPL_{max}$ obtained from the LPL rotational measurement at 513 nm, as shown in Figure 4a. Likewise, the true CPL measurement of an enantiomeric crystal was conducted using the aforementioned procedure for the solid CPL sample. A mirror image of the true CPL signal of the benzil isomers was obtained, as shown in Figure 4b. The validity of the CPL spectra was demonstrated by the fact that the absolute g_{lum} values were nearly identical (2.2×10^{-3} and 2.5×10^{-3}) in the enantiomeric crystals and in good agreement with the previously reported value (3×10^{-3}) [40].

Conclusion

In this paper, we discussed the principles and applications of chiroptical (CD and CPL) measurements for supramolecular samples having optical anisotropies and presented many of the advances achieved by using the devised Stokes–Mueller matrix analysis for optically anisotropic systems. Commercially available CD and CPL spectrophotometers are restricted to optically isotropic samples. To obtain true chiroptical signals, it is essential to estimate the nonchiral linearly polarized components that are mixed into the measured raw signal and to obtain the true chiroptical signal by a suitable analytical method. Aiming to create a new field of chiral chemistry for optically anisotropic systems, versatile chiroptical spectrophotometers have been designed and constructed, and an analytical procedure based on the Stokes–Mueller matrix has been devised. These advancements are invaluable for measuring the true CD and CPL spectra of optically active samples having macroscopic anisotropies in the condensed phase or solution and solid states.

We expect that further improvements will be made as methods are investigated to routinely perform chiroptical spectroscopies based on polarization modulation techniques as rapidly as possible without disturbances from the artifacts resulting from the interaction between the macroscopic anisotropies of a sample and the nonideal optical and electrical elements required for its measurement.

Acknowledgements We thank emeritus Prof. Y Shindo and Prof. R Kuroda for their helpful discussions and support and Mr. H Hayakawa and Dr. M Watanabe of JASCO Co., Ltd. for technical assistance. This work was supported by a Grant-in-Aid for Scientific Research, Grant Nos. 25870996 and 15K04610, from the Japan Society for the Promotion of Science and a research fund from System Instruments Co., Ltd.

Compliance with ethical standards

Conflict of interest The authors declare that they have no conflict of interest.

References

1. Nafie LA. Vibrational optical activity: principles and applications. 1st ed. Chichester, UK: Wiley; 2011.
2. Bilotti I, Biscarini P, Ferranti F, Castiglioni E, Kuroda R. Reflectance circular dichroism of solid-state chiral coordination compounds. Chirality. 2002;14:750–6.
3. Barron LD, Bogaard MP, Buckingham AD. Raman scattering of circularly polarized light by optically active molecules. J Am Chem Soc. 1973;95:603–5.
4. Elkins HB, Kuhn W. The circular dichroism of optically active β-octyl nitrite in the vapor state. J Am Chem Soc. 1935;57:296–9.
5. Samoilov BN. Absorption and luminescence spectra of uranyl salts at temperatures of liquid helium. J Exp Theor Phys. 1948;18:1030–40.
6. Jensen HP, Schellman JA, Troxell T. Modulation techniques in polarization spectroscopy. Appl Spectrosc. 1978;32:192–200.
7. Dekkers HPJM. Circularly polarized luminescence: A probe for chirality in the excited state. In: Berova N, Nakanishi K, Woody WR, editors. Circular dichroism: principles and applications. 2nd ed. Ch. 7. Wiley-VCH: New York; 2000. p. 185–215.
8. Harada N, Nakanishi K. Circular dichroic spectroscopy: exciton coupling in organic stereochemistry. Mill Valley, CA: University Science Books; 1983.
9. Matile S, Berova N, Nakanishi K, Novkova S, Philipova I, Blagoev B. Porphyrins: powerful chromophores for structural studies by exciton-coupled circular dichroism. J Am Chem Soc. 1995;117:7021–2.
10. Sisido M, Egusa S, Okamoto A, Imanishi Y. Circularly polarized fluorescence of aromatic poly(α-amino acids). J Am Chem Soc. 1983;105:3351–2.
11. McCaffery AJ, Mason SF, Norman BJ. Optical rotatory power of co-ordination compounds. Part XII. Spectroscopic and configurational assignments for the tris-bipyridyl and -phenanthroline complexes of the di- and tri-valent iron-group metal ions. J Chem Soc A. 1969;0:1428–41.
12. Hu H-Y, Li Q, Cheng H-C, Du H-N. β-Sheet structure formation of proteins in solid state as revealed by circular dichroism spectroscopy. Biopolymers. 2001;62:15–21.
13. Shindo Y, Nishio M. The effect of linear anisotropies on the CD spectrum: is it true that the oriented polyvinylalcohol film has a magic chiral domain inducing optical activity in achiral molecules? Biopolymers. 1990;30:25–31.
14. Gottarelli G, Lena S, Masiero S, Pieraccini S, Spada GP. The use of circular dichroism spectroscopy for studying the chiral molecular self-assembly: an overview. Chirality. 2008;20:471–85.
15. Saeva FD, Wysocki JJ. Induced circular dichroism in cholesteric liquid crystals. J Am Chem Soc. 1971;93:5928–9.
16. Kuball, H-G, Höfer, T. In: Kitzerow H, Bahr C, editors. From a chiral molecule to a chiral anisotropic phase. Chirality in liquid crystals (partially ordered systems). Ch. 3. New York: Springer; 2001. p. 67–100.
17. Satrijo A, Mesker SCJ, Swager TM. Probing a conjugated polymer's transfer of organization-dependent properties from solutions to films. J Am Chem Soc. 2006;128:9030–1.
18. Schellman J, Jensen HP. Optical spectroscopy of oriented molecules. Chem Rev. 1987;87:1359–99.
19. Yang D, Duan P, Zhang L, Liu M. Chirality and energy transfer amplified circularly polarized luminescence in composite nanohelix. Nat Commun. 2017;8:15727.
20. Norden B. Linear and circular dichroism of polymeric pseudoisocyanine. J Phys Chem. 1977;81:151–9.
21. Dekkers HPJM, Moraal PF, Timper JM, Riehl JP. Optical artifacts in circularly polarized luminescence spectroscopy. Appl Spectrosc. 1985;39:818–21.
22. Shindo Y, Ohmi Y. Problems of CD spectrometers. 3. Critical comments on liquid crystal induced circular dichroism. J Am Chem Soc. 1985;107:91–97.
23. Shindo Y, Oda Y. Mueller matrix approach to fluorescence spectroscopy. Part I: Mueller matrix expressions for fluorescent samples and their application to problems of circularly polarized emission spectroscopy. Appl Spectrosc. 1992;46:1251–9.
24. Shindo Y, Nakagawa M. Circular dichroism measurements. I. Calibration of a circular dichroism spectrometer. Rev Sci Instrum. 1985;56:32–39.
25. Mueller H. The foundation of optics. J Opt Soc Am. 1948;38:661–3.
26. Kuroda R, Harada T, Shindo Y. A solid-state dedicated circular dichroism spectrophotometer: development and application. Rev Sci Instrum. 2001;72:3802–10.
27. Shindo Y, Kani K, Horinaka J, Kuroda R, Harada T. The application of polarization modulation method to investigate the optical homogeneity of polymer films. J Plast Film Sheet. 2001;17:164–83.
28. Harada T, Hayakawa H, Kuroda R. Vertical-type chiroptical spectrophotometer (I): instrumentation and application to diffuse reflectance circular dichroism measurement. Rev Sci Instrum. 2008;79:073103.
29. Harada T, Miyoshi Y, Kuroda R. High performance diffuse reflectance circular dichroism spectrophotometer. Rev Sci Instrum. 2009;80:046101.
30. Kuroda R, Harada T. In: Berova N, Polavarapu PL, Nakanishi K, Woody RW, editors. Comprehensive chiroptical spectroscopy: instrumentation, methodologies, and theoretical simulations. Ch. 4. New York: Wiley; 2012. p. 91–113.
31. Gorecki M, Zinna F, Biver T, Bari DL. Induced circularly polarized luminescence for revealing DNA binding with fluorescent dyes. J Pharm Biomed Anal. 2017;144:6–11.
32. Yeom J, Yeom B, Chan H, Smith KW, Dominguez-Medina S, Bahng JH, Zhao G, Chang W-S, Chang S-J, Chuvilin A, Melnikau D, Rogach AL, Zhang P, Link S, Kral P, Kotov NA. Chiral templating of self-assembling nanostructures by circularly polarized light. Nat Mater. 2015;14:66–72.
33. Kumar J, Nakashima T, Kawai T. Circularly polarized luminescence in chiral molecules and supramolecular assemblies. J Phys Chem Lett. 2015;6:3445–52.
34. Chen SH, Katsis D, Schmid AW, Mastrangelo JC, Tsutsui T, Blanton TN. Circularly polarized light generated by photoexcitation of luminophores in glassy liquid-crystal films. Nature. 1999;397:506–8.
35. Furumi S. Self-assembled organic and polymer photonic crystals for laser applications. Polym J. 2013;45:579–93.
36. Watanabe K, Akagi K. Helically assembled π-conjugated polymers with circularly polarized luminescence. Sci Technol Adv Mater. 2014;15:044203.
37. Hayasaka H, Miyashita T, Tamura K, Akagi K. Helically π-stacked conjugated polymers bearing photoresponsive and chiral

moieties in side chains: reversible photoisomerization-enforced switching between emission and quenching of circularly polarized fluorescence. Adv Funct Mater. 2010;20:1243–50.
38. Peeters E, Christiaans MPT, Janssen RAJ, Schoo HFM, Dekkers HPJP, Meijer EW. Circularly polarized electroluminescence from a polymer light-emitting diode. J Am Chem Soc. 1997;119:9909–10.
39. Ikeda H, Nishizawa N, Nishibayashi K, Munekata H. Circularly polarized light detector based on ferromagnet/semiconductor junctions. J Magn Soc Jpn. 2014;38:147–50.
40. Harada T, Kuroda R, Moriyama H. Solid-state circularly polarized luminescence measurements: theoretical analysis. Chem Phys Lett. 2012;530:126–31.
41. Harada T, Hayakawa H, Watanabe M, Takamoto M. A solid-state dedicated circularly polarized luminescence spectrophotometer: development and application. Rev Sci Instrum. 2016;87:075102.
42. Bile EG, Cortelazzo-Polisini E, Denicourt-Nowicki A, Sassine R, Launay F, Roucoux A. Chiral ammonium-capped rhodium(0) nanocatalysts: synthesis, characterization, and advances in asymmetric hydrogenation in neat water. ChemSusChem. 2012;5:91–101.
43. Stroke GW. An introduction to coherent optics and holography. 2nd edn. New York: Academic Press; 1969.
44. Shurcliff WA. Polarized light production and use. Cambridge, MA: Harvard University Press; 1962.
45. Go N. Optical activity of anisotropic solutions. II. J Phys Soc Jpn. 1967;23:88–97.
46. Schellman JA. In: Samori B, Thulstrup EW, editors. Polarization Modulation Spectroscopy. Polarized spectroscopy of ordered systems. Dordrecht: Kluwer Academic Publishers; 1988. p. 231–74.
47. Harada T, Kurihara M, Kuroda R, Moriyama H. On–off switching of the novel thermochromic chiroptical behavior of pseudoisocyanine driven by association/dissociation. Chem Lett. 2012;41:1442–4.
48. Oda M, Nothofer H-G, Lieser G, Scherf U, Meskers SCJ, Neher D. Circularly polarized electroluminescence from liquid-crystalline chiral polyfluorenes. Adv Mater. 2000;12:362–5.
49. Palsson L-O, Vaughan HL, Monkman AP. Polarized optical spectroscopy applied to investigate two poly(phenylene-vinylene) polymers with different side chain structures. J Chem Phys. 2006;125:164701.
50. Harada T, Kuroda R. Circular dichroism measurement of a protein in dried thin films. Chem Lett. 2002;31:326–7.
51. Harada T, Kuroda R. CD measurements of β-amyloid (1–40) and (1–42) in the condensed phase. Biopolymers. 2011;95:127–34.
52. Babenko V, Harada T, Yagi H, Goto Y, Kuroda R, Bzwolak W. Chiral superstructures of insulin amyloid fibrils. Chirality. 2011;23:638–46.
53. Victor VV, Harada T, Inoue Y, Kuroda R. Phase-sensitive supramolecular chirogenesis in Bisporphyrin system. Angew Chem Int Ed. 2003;41:1387–1381.
54. Okayasu Y, Yuasa J. Evaluation of circularly polarized luminescence in a chiral lanthanide ensemble. Mol Syst Des Eng. 2018;3:66–72.
55. Tsumatori H, Harada T, Yuasa J, Hasegawa Y, Kawai T. Circularly polarized light from chiral lanthanide(III) complexes in single crystals. Appl Phys Express. 2011;4:011601–3.
56. Harada T, Moriyama H, Takahashi H, Umemura K, Yokota H, Kawakami Y, Mishima K. Spectroscopic characterization of supramolecular chiral porphyrin homoassociates at the air–water interface. Appl Spectrosc. 2013;68:1235–40.
57. Harada T, Kajiyama N, Ishizaka K, Toyofuku R, Izumi K, Umemura K, Imai Y, Taniguchi N, Mishima K. Plasmon resonance-enhanced circularly polarized luminescence of self-assembled meso-tetrakis(4-sulfonatophenyl)porphyrin–surfactant complexes in interaction with Ag nanoparticles. Chem Commun. 2014;50:11169–72.
58. El-Hachemi Z, Arteage O, Canillas A, Crusats J, Escudero C, Kuroda R, Harada T, Rosa M, Ribo JM. On the mechano-chiral effect of vertical flows on the dichroic spectra of 5-phenyl-10,15,20-tris(4-sulfonatophenyl)porphyrin J-aggregates. Chem Eur J. 2008;14:6438–43.
59. Ohno O, Kaizu Y, Kobayashi H. J-aggregate formation of a water-soluble porphyrin in acidic aqueous media. J Chem Phys. 1993;99:4128–38.
60. Fujii Y, Tsukahara Y, Wada Y. pH-dependent reversible switching of fluorescence of water-soluble porphyrin adsorbed on mesoporous TiO_2 film. Bull Chem Soc Jpn. 2006;79:561–8.
61. Harada T, Shindo Y, Kuroda R. Crystal chirality of the non-chiral inorganic salt, α-$Ni(H_2O)_6{\cdot}SO_4$. Chem Phys Lett. 2002;360:217–22.
62. Murata K, Aoki M, Suzuki T, Hatada T, Kawabata H, Komori T, Ohseto F, Ueda K, Shinkai S. Thermal and light control of the sol-gel phase transition in cholesterol-based organic gels. Novel helical aggregation modes as detected by circular dichroism and electron microscopic observation. J Am Chem Soc. 1994;116:6664–76.
63. Ardhammar M, Lincoln P, Rodger A, Norden B. Absolute configuration and electronic state properties of light-switch complex $[Ru(phen)_2dppz]^{2+}$ deduced from oriented circular dichroism in a lamellar liquid crystal host. Chem Phys Lett. 2002;354:44–50.